



POLITECNICO
DI TORINO

POLITECNICO DI TORINO

Master degree course in Physics of complex systems

Master Degree Thesis

Optical analogue of self-gravitating systems

Supervisors

Prof. Bruno Marcos
Prof. Alessandro Pelizzola

Candidate

Martino LOVISETTO
Matricola: 238816

ACADEMIC YEAR 2017-2018

Summary

Many interactions in nature are long range. As long range interactions, we refer to those in which parts of the system far away from each other interact considerably. An historical example of such systems are stars inside a galaxy or globular clusters. Typically, in such a system, a star is subjected to a force dominated by the ensemble of the other stars (long range) rather than, for example, the neighboring ones (short range). As a consequence, one expects a very different behavior (and often counter-intuitive) compared to what happens in the short-range interacting regime usually encountered in statistical physics textbooks. For example, in the thermodynamic equilibrium, there is nonequivalence of ensembles [1] or a possible apparition of negative specific heat in the micro-canonical ensemble [2]. The macroscopic dynamics is also very different: starting from arbitrary initial conditions, the system forms rapidly a quasi-stationary state (like a galaxy) and then relaxes towards thermodynamic equilibrium. Recently, it has been observed [3] that a laser beam propagating through a nonlinear, nonlocal medium presents a behavior very similar to the formation of a quasi-stationary state of self-gravitating bosons in the non-relativistic regime [4], which is a serious candidate for dark matter in the halos of galaxies.

The purpose of this internship, is studying theoretically and numerically such an optical analogue of a self-gravitating system. The targeted objectives are listed below.

1. Full description of the analogy between self-gravitating systems and nonlinear optical propagation, together with a variational approach in order to derive an analytical solution of the equation.
2. Study the evolution of the system for various initial conditions by writing a code to solve the Schrödinger-Newton equation [5].
3. Comparisons between theory and simulations oriented to the realisation of the optimal experimental procedure in the optical framework.

Acknowledgements

I would like to thank my supervisor, Bruno Marcos, for the help he provided me with during the internship work. Moreover I would like to thank as well Claire Michel and Matthieu Bellec from the INPHYNI lab who are part of the experimental side of the project. Finally I'm also grateful to Didier Clamond from LJAD lab who helped me with the more technical mathematical aspects.

Contents

List of Tables	6
List of Figures	7
I Theoretical Aspects	9
1 Full Description Of The Mathematical Analogy	11
1.1 The Newton-Schrödinger equation	11
1.1.1 Application of NSE	12
1.1.2 Derivation of NSE	12
1.2 The Paraxial-Helmholtz equation	13
1.2.1 Derivation of PHE	13
1.2.2 Experimental reproduction of the PHE system	15
1.3 Analogy between the two frameworks	16
1.3.1 Dimensionless form	17
2 Hydrodynamical Picture	19
2.1 Madelung Transformation	19
2.2 Variational approach	20
2.2.1 Gaussian ansatz	21
II Numerical simulations	25
3 Algorithm description	27
3.1 Split-Step method	27
3.1.1 Error	28
3.2 Spectral method	30
3.2.1 Fast Fourier Transform	30

4	Results for different initial conditions	33
4.1	Parameters value	33
4.2	Conserved quantities	34
4.3	Single beam initial condition	35
4.3.1	Variational model comparison	36
4.4	Double beam initial condition	37
5	Quasi-stationary state	39
5.1	Virial theorem	39
5.1.1	Classical Virial theorem	39
5.1.2	Quantum Virial theorem	40
5.2	Comparison with simulations	40
5.2.1	Multiscale nature of the problem	43
5.3	Study of the stationarity in time	44
5.3.1	Numerical solution	44
6	Phase-space picture	49
6.1	Classical limit of NSE	49
6.1.1	Comparison with Planck constant	49
6.1.2	Role of the quantum pressure	50
6.2	Husimi distribution	51
6.2.1	Numerical evaluation and plots	52
	Appendices	57
A	Details of the PHE derivation	59
B	Evaluating Virial integral	61
	Bibliography	63

List of Tables

4.1	Experimental Parameters	34
5.1	Percentage discrepancy Virial theorem	41

List of Figures

1.1	Experimental setup	16
2.1	Initial potential	23
4.1	Energy conservation	35
4.2	Power conservation	35
4.3	Single Gaussian small z	36
4.4	Single Gaussian large z	36
4.5	Variational model comparison	37
4.6	Double Gaussian	38
5.1	Virial theorem plots	42
5.2	Time stationarity plots	47
6.1	Quantum pressure comparison	51
6.2	Husimi distribution plots	53

Part I

Theoretical Aspects

Chapter 1

Full Description Of The Mathematical Analogy

In this chapter we introduce the analogy we relied on and the equations over which it is based: the Newton-Schrödinger equation and the Paraxial-Helmholtz equation. We first describe them separately, then we explain under which conditions the mathematical analogy is perfectly valid.

1.1 The Newton-Schrödinger equation

The Newton-Schrödinger equation (NSE) describes the evolution of a distribution of mass m , associated with a wave function ψ (interpreted as the mass density) and subjected to the classical, i.e. Newtonian, gravitational field ϕ generated by itself:

$$i\hbar\frac{\partial\psi}{\partial t} + \frac{\hbar^2}{2m}\nabla^2\psi + m\phi\psi = 0 \quad (1.1)$$

$$\nabla^2\phi = -4\pi Gm|\psi|^2. \quad (1.2)$$

Where G is the gravitational constant, ∇^2 is the 3-dimensional Laplace operator, \hbar the reduced Planck constant and m the mass of the particles.

Physical systems like this one, which interact through their own gravitational field, are usually called self-gravitating systems.

Even though the details about the gravitational side of the analogy are not in the purposes of this work, we just briefly describe in the next two sections the possible applications of this equation together with its derivation.

1.1.1 Application of NSE

This equation can be used for example to describe dark matter [6]. Even though exploiting a quantum framework to describe an astrophysical system could seem illogic, there are at least a couple of good reasons to do that. The first one is that, often, taking the $\hbar \rightarrow 0$ limit of the Schrödinger equation is actually more convenient, as with this technique there is the advantage of working in a 3-dimensional space (i.e. the positions space for the wave function) instead of the 6-dimensional one, given by the classical phase-space distribution of the system. The second reason is due to the fact that the quantum approach allows to explain, via the Heisenberg uncertainty relation, the homogeneous distribution of dark matter near the centre of galaxies [7], while the classical picture, which relies on the Vlasov-Poisson equation, fails in justifying this feature. In this model, also known as ψDM [7], dark matter particles are interpreted as bosonic particles whose mass is very small $m_b \approx 10^{-23} eV$ and with a very large position indetermination, $\Delta x \approx 1 kpc$.

1.1.2 Derivation of NSE

It is possible to derive NSE from the Klein-Gordon equation coupled with the weak field limit of general relativity [8]. In this limit, gravity can be described in a classical way, according to the Newtonian potential:

$$\hbar^2[-(1 - 2\Phi)\partial_t^2 + c^2(1 + 2\Phi)\nabla^2]\Psi - m^2c^4\Phi = 0 \quad (1.3)$$

$$\nabla^2\Phi = -4\pi Gm\Psi^*\Psi$$

since the metric tensor components are given by:

$$g_{00} = (1 - 2\Phi) \quad g_{ij} = (1 - 2\Phi)\delta_{ij} \quad i, j = 1, 2, 3.$$

If we assume that $\Phi \ll 1$ and that Φ^2 is negligible, we can proceed with the usual ansatz often exploited in quantum field theory to get the non-relativistic limit [9]:

$$\Psi = \psi e^{-\frac{imc^2}{\hbar}t}. \quad (1.4)$$

By neglecting $\mathcal{O}(c^{-2})$ terms, plugging (1.4) into (1.3) leads to:

$$i\hbar(1 - 2\Phi)\partial_t\psi = -(1 + 2\Phi)\frac{\hbar^2}{2m}\nabla^2\psi + mc^2.$$

Which corresponds, if one neglect $\psi\Phi$ products, to the regular NSE.

1.2 The Paraxial-Helmholtz equation

The Paraxial-Helmholtz equation (PHE) describes the evolution of the amplitude ε of an optical beam propagating through a nonlocal medium:

$$i\frac{\partial\varepsilon}{\partial z} + \frac{1}{2k}\nabla_{\perp}^2\varepsilon + k_0\Delta n\varepsilon = 0 \quad (1.5)$$

$$\nabla_{\perp}^2\Delta n = -\frac{\alpha\beta}{\kappa}|\varepsilon|^2 \quad (1.6)$$

where k and k_0 are the wave-numbers of the beam respectively inside the medium and in void, ∇_{\perp}^2 is the 2-dimensional transverse Laplace operator, z is the propagation direction of the beam, β is the medium thermo-optic coefficient, κ the thermal conductivity and α the absorption coefficient.

In particular, we are considering the case of a medium characterized by a thermo-optical nonlinearity, which links the variation of the refractive index Δn of the medium itself with the intensity of the beam $|\varepsilon|^2$. As we shall see next, equation (1.6) is essentially a stationary heat-like equation, where the heat source is associated with the self-focusing laser increasing the temperature of the medium while propagating through it.

1.2.1 Derivation of PHE

Equation (1.5) can be derived directly from Maxwell equations (ME) under proper approximations [10]. We consider the case of a continuous wave beam propagating inside a nonlinear optical medium. In such a medium, for the electric field vector \vec{E} we rely on the following equation, which is a direct consequence of ME:

$$\nabla\vec{E} - \frac{1}{c^2}\frac{\partial^2\vec{E}}{\partial t^2} = \frac{1}{\epsilon^2}\frac{\partial^2\vec{P}}{\partial t^2} \quad (1.7)$$

where c is the speed of light in the medium we consider and ϵ its permittivity. The induced polarization \vec{P} consists of two parts such that:

$$\vec{P}(\vec{r}, t) = \vec{P}_L(\vec{r}, t) + \vec{P}_{NL}(\vec{r}, t)$$

where the linear part $\vec{P}_L(\vec{r}, t)$ and the nonlinear part $\vec{P}_{NL}(\vec{r}, t)$ are related to the electric field through the susceptibility first and third tensors, i.e. $\chi^{(1)}$ and $\chi^{(3)}$:

$$\vec{P}_L(\vec{r}, t) = \epsilon \int_{-\infty}^{\infty} \chi^{(1)}(t-t') \cdot \vec{E}(\vec{r}, t') dt'$$

$$\begin{aligned} \vec{P}_{NL}(\vec{r}, t) = & \epsilon \iiint_{-\infty}^{\infty} \chi^{(3)}(t - t_1, t - t_2, t - t_3) \times \\ & \times \vec{E}(\vec{r}, t_1) \vec{E}(\vec{r}, t_2) \vec{E}(\vec{r}, t_3) dt_1 dt_2 dt_3. \end{aligned} \quad (1.8)$$

In order to reduce these equations to a more treatable form, we rely on several assumptions, listed and justified below.

- The nonlinear response is assumed to be instantaneous so that the time dependence of $\chi^{(3)}$ is given by the product of three delta functions of the form $\delta(t - t_i)$. Than Eq. (1.8) reduces to:

$$\vec{P}_{NL}(\vec{r}, t) = \epsilon \chi^{(3)} \vec{E}(\vec{r}, t) \vec{E}(\vec{r}, t) \vec{E}(\vec{r}, t).$$

The assumption of instantaneous nonlinear response corresponds to neglecting the contribution of molecular vibrations to $\chi^{(3)}$ whose detection requires a resolution in wavelength much higher than the one typically employed in this framework.

- \vec{P}_{NL} can be treated as a small perturbation to \vec{P}_L because nonlinear changes in the refractive index are $\frac{\Delta n}{n} < 10^{-6}$ in practice.
- The optical field is assumed to maintain its polarization along the medium so that a scalar approach can be used, this is valid in our case since we are interested into isotropic materials.
- We make the ansatz:

$$\vec{E}(\vec{r}, t) = \frac{1}{2} \hat{p} [A(\vec{r}) e^{ikz} e^{-i\omega_0 t} + c.c.]$$

where ω_0 is the carrier frequency, \hat{p} is the polarization unit vector, $k = k_0 n_b = \frac{2\pi n_b}{\lambda}$ is the propagation constant in terms of the optical wavelength $\lambda = \frac{2\pi c}{\omega_0}$, *c.c.* denotes the complex conjugated and $A(\vec{r}) e^{ikz}$ is called envelope function. The polarization components $\vec{P}_L(\vec{r}, t)$ and $\vec{P}_{NL}(\vec{r}, t)$ can also be expressed in a similar way.

- We rely on the slowly varying envelope approximation [11] which means that within a distance $\Delta z = \lambda$, the change ΔA is much smaller than A itself. Quantitatively this implies that:

$$\begin{aligned} \Delta A \ll A & \Leftrightarrow \Delta z \ll \lambda \Rightarrow \\ & \Rightarrow \frac{\partial A}{\partial z} \ll \frac{A}{\lambda} = \frac{Ak}{2\pi} \Rightarrow \\ & \Rightarrow \frac{\partial A}{\partial z} \ll kA, \quad \frac{\partial^2 A}{\partial z^2} \ll k^2 A. \end{aligned}$$

- The thermo-optical nonlinearity can be included by assuming that the refractive index varies with temperature [12] according to:

$$n = n_b + \frac{dn}{dT} \tilde{T}_l$$

where \tilde{T}_l represents the laser induced change in temperature. The quantity $\frac{dn}{dT}$ is a constant called the medium thermo-optic coefficient. By assuming that \tilde{T}_l obeys to the heat-transport equation, we have:

$$\rho_0 C \frac{\partial \tilde{T}_l}{\partial t} - \kappa \nabla^2 \tilde{T}_l = \alpha I \quad (1.9)$$

which in the stationary regime, coincides with Eq. (1.6). Here $\rho_0 C$ denotes the heat capacity per unit volume and $I = |\varepsilon|^2$ the intensity of the beam.

- Since, according to our ansatz solution, we are working with monochromatic waves, in Fourier space the dielectric constant and the refractive index are proportional to each other (see Appendix A). This means that the nonlinear part of the refractive index, comes from the nonlinear part of \vec{P} .

By taking into account these assumptions, with some algebraic manipulations, plugging the ansatz for \vec{E} and \vec{P} into (1.7) leads to the Paraxial Helmholtz equation:

$$2ik \frac{\partial A}{\partial z} + \nabla_{\perp}^2 A + 2kk_0 \Delta n(I) A = 0$$

which clearly corresponds to Eq. (1.5).

1.2.2 Experimental reproduction of the PHE system

Even though this internship is essentially a theoretical and numerical work, a collaboration with INPHYNI lab is planned in order to perform in the future an experimental realisation of the PHE system. Therefore we would like to say something about how in practice one could reproduce the optical framework of the analogy. As shown in figure 1.1, the laser, coming from a monochromatic source, propagates through a lead glass. Notice that since in our analogy the propagation direction is mapped into time (this will be better explained in the next section), it is important to use materials with a

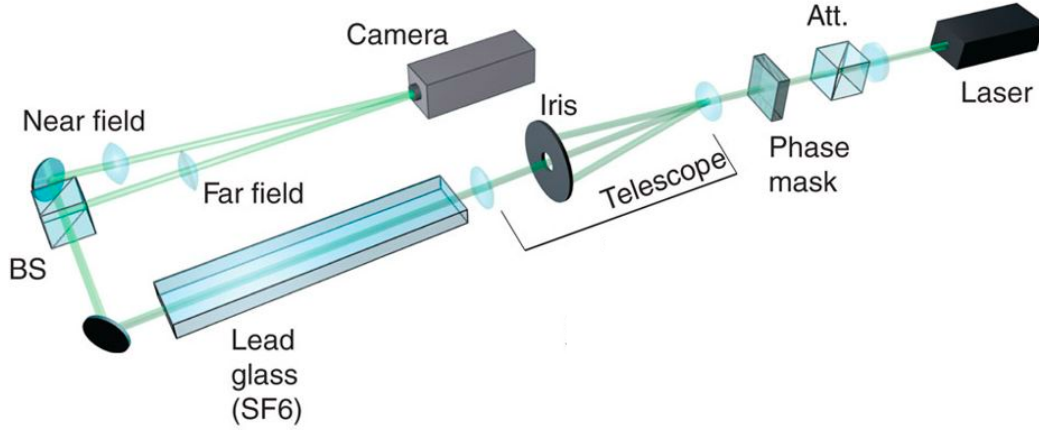


Figure 1.1. Example of a typical experimental setup employed to simulate PHE systems.

bar-like geometry: then longer the material is, then larger is the time-scale which can be explored through the analogy.

However, since there are some technical limits in the realisation of such very long media, as we shall see next, we will exploit the manipulation of the input laser and of its power, in order to explore larger values of time in the gravitational framework. A good control over the initial condition is ensured by the phase mask which is characterized by 1000×1200 pixels. This means that we are able to select and manipulate phase and intensity in the optical beam with a very high precision. Moreover we are able to work within a range of power which approximately goes from $1W$ to $10W$.

1.3 Analogy between the two frameworks

If we consider a 2-dimensional slice of the NSE system, namely:

$$\nabla = \nabla_{\perp}^2 = \frac{\partial^2}{\partial x^2} + \frac{\partial^2}{\partial y^2}$$

and if we do the mapping:

$$z \leftrightarrow t$$

then apart for constants NSE and PHE are perfectly equivalent under a mathematical point of view [13]. The advantage of this is that, while on the

one hand the optical system can easily be reproduced with an experiment in a lab, on the other hand the NSE system has been studied strictly theoretically. Therefore one can exploit this analogy in order to achieve a better understanding of gravitational systems, which are often harder to directly observe.

1.3.1 Dimensionless form

Now we make our equations dimensionless, we do it by considering the most general form:

$$\begin{aligned} i a_1 \frac{\partial \tilde{\psi}}{\partial \tilde{z}} + \frac{a_2}{2} \tilde{\nabla}^2 \tilde{\psi} - a_3 \tilde{V} \tilde{\psi} &= 0 \\ \tilde{\nabla}^2 \tilde{V} &= a_4 |\tilde{\psi}|^2 \end{aligned} \quad (1.10)$$

where the $a_i > 0$ are constants and tilded quantities correspond to dimensional variables. The dimensionless form is achieved by choosing the following scales:

$$\begin{aligned} \tilde{z} &= \frac{g a_1}{a_2 a_3 a_4} z, & (\tilde{x}, \tilde{y}) &= \left(\frac{g}{a_3 a_4}\right)^{\frac{1}{2}} (x, y) \\ \tilde{\psi} &= \left(\frac{a_2 a_3 a_4}{g}\right)^{\frac{1}{2}} \psi, & \tilde{V} &= \frac{a_2 a_4}{g} V. \end{aligned} \quad (1.11)$$

In particular, by plugging Eq. (1.11) into (1.10) we get:

$$\begin{aligned} i \frac{\partial \psi}{\partial z} + \frac{1}{2} \nabla^2 \psi - V \psi &= 0 \\ \nabla^2 V &= g |\psi|^2 \end{aligned} \quad (1.12)$$

where the constant $g > 0$ can be fixed to any positive value. Notice that a direct comparison with eq (1.2) and (1.6) would imply $V = -\phi$.

Chapter 2

Hydrodynamical Picture

In this chapter we describe a variational approach to the analytical solution of the equations, this approach relies on a hydrodynamical picture and a gaussian ansatz. The results obtained will be useful for later comparisons with the numerics. In what follows we will use $g = 1$ referring to eq (1.12), therefore:

$$\begin{aligned} i\frac{\partial\psi}{\partial z} + \frac{1}{2}\nabla^2\psi - V\psi &= 0 \\ \nabla^2 V &= |\psi|^2. \end{aligned} \tag{2.1}$$

2.1 Madelung Transformation

We start by writing the wave function in Eq. (2.1) using what in the literature goes under the name of Madelung transformation [14]:

$$\psi(\vec{r}, t) = \sqrt{\rho(\vec{r}, t)}e^{iS(\vec{r}, t)} \tag{2.2}$$

where $\rho(\vec{r}, t)$ and $S(\vec{r}, t)$ are respectively the amplitude and the phase of the wave function.

Plugging (2.2) in (2.1) leads to:

$$i\frac{1}{2\sqrt{\rho}}\frac{\partial\rho}{\partial t} + \sqrt{\rho}\frac{\partial S}{\partial t} + \frac{1}{2}\left(\nabla^2\sqrt{\rho} + \frac{i}{\sqrt{\rho}}\nabla\rho\cdot\nabla S + i\nabla^2 S\sqrt{\rho} - |\nabla S|^2\sqrt{\rho}\right) - V\sqrt{\rho} = 0 \tag{2.3}$$

$$\nabla^2 V = \rho. \tag{2.4}$$

By direct comparison of real and imaginary part of both sides of equation (2.3), we get two equations:

$$\begin{aligned} \frac{\partial \rho}{\partial t} + \nabla \rho \cdot \nabla S + \nabla^2 S \rho &= 0 \\ \frac{\partial S}{\partial t} + \frac{1}{2} \left(\frac{\nabla^2 \sqrt{\rho}}{\sqrt{\rho}} - |\nabla S|^2 \right) - V &= 0. \end{aligned} \quad (2.5)$$

If we introduce the quantity $\vec{u} = \nabla S$ and apply the gradient to Eq. (2.5), then we get:

$$\begin{aligned} \frac{\partial \rho}{\partial t} + \nabla(\rho \cdot \vec{u}) &= 0 \\ \frac{\partial \vec{u}}{\partial t} + \vec{u}(\nabla \cdot \vec{u}) &= -\nabla V + \frac{1}{2} \nabla \left(\frac{\nabla^2 \sqrt{\rho}}{\sqrt{\rho}} \right). \end{aligned} \quad (2.6)$$

$$(2.7)$$

We have just proved how the NSE system is completely equivalent to a hydrodynamical system, as 2.6 and 2.7 represent respectively the continuity and the Euler equation for a fluid with density ρ , velocity field \vec{u} and subjected to a potential V , given by Eq. (2.4). The $\frac{1}{2} \nabla \left(\frac{\nabla^2 \sqrt{\rho}}{\sqrt{\rho}} \right)$ term can be interpreted as a pressure. In particular, since it comes from the kinetic energy in the quantum frame, we can interpret it as a kinetic pressure due to Heisenberg uncertainty relation.

2.2 Variational approach

It is convenient at this point, to derive a Lagrangian density associated with the equations of the system:

$$\begin{aligned} \frac{\partial \rho}{\partial t} + \nabla(\rho \cdot \vec{u}) &= 0 \\ \frac{\partial \vec{u}}{\partial t} + \vec{u}(\nabla \cdot \vec{u}) &= -\nabla V + \frac{1}{2} \nabla \left(\frac{\nabla^2 \sqrt{\rho}}{\sqrt{\rho}} \right) \\ \nabla^2 V &= \rho. \end{aligned} \quad (2.8)$$

To do that, in the spirit of what in the literature is usually done in $3d$ [15], we write a Lagrangian density and check that it actually gives back Eq. (2.8) when we write the equations of motion associated with it. The Lagrangian density we refer to is:

$$\mathcal{L}(\rho, S, V) = \frac{\rho}{2}(\nabla S)^2 + \rho \frac{\partial S}{\partial t} + \frac{|\nabla \rho|^2}{8\rho} + \frac{|\nabla V|^2}{2} + \rho V. \quad (2.9)$$

Indeed when we write the Euler-Lagrange equations associated with \mathcal{L} , by paying attention to the fact that we should consider derivatives with respect to space-time like it is usually done in quantum field theory, we get:

$$\begin{aligned} \frac{\partial \mathcal{L}}{\partial \rho} &= \nabla \cdot \left(\frac{\partial \mathcal{L}}{\partial(\nabla \rho)} \right) + \frac{\partial}{\partial t} \left(\frac{\partial \mathcal{L}}{\partial(\frac{\partial \rho}{\partial t})} \right) \\ \frac{\partial \mathcal{L}}{\partial S} &= \nabla \cdot \left(\frac{\partial \mathcal{L}}{\partial(\nabla S)} \right) + \frac{\partial}{\partial t} \left(\frac{\partial \mathcal{L}}{\partial(\frac{\partial S}{\partial t})} \right) \\ \frac{\partial \mathcal{L}}{\partial V} &= \nabla \cdot \left(\frac{\partial \mathcal{L}}{\partial(\nabla V)} \right) + \frac{\partial}{\partial t} \left(\frac{\partial \mathcal{L}}{\partial(\frac{\partial V}{\partial t})} \right). \end{aligned} \quad (2.10)$$

The first one gives back Euler equation, the second one gives back continuity equation and the third one, Poisson equation.

2.2.1 Gaussian ansatz

We now try to explicitly solve Eq. (2.10), through a gaussian ansatz for the density ρ . From now on, we focus on the optical framework, considering two spatial dimensions and mapping time into z , for simplicity of notation though, instead of using r_\perp , we still denote as $r = \sqrt{x^2 + y^2}$ the radial distance from the origin in the transverse plan.

The ansatz we make deals with a Gaussian in the transverse plane with a z -dependent width:

$$\rho(\vec{r}, z) = \mathcal{N} e^{-\frac{r^2}{R(z)^2}} \quad (2.11)$$

where \mathcal{N} is a normalization constant. The value of \mathcal{N} which normalizes the density to unity in the transverse plane is:

$$\iint \rho(\vec{r}, z) dx dy = 1 \quad \Leftrightarrow \quad \mathcal{N} = \frac{1}{\pi R(z)^2}$$

which depends on the width $R(z)$.

Thanks to this ansatz we are now able to analytically solve Eq. (2.4), by exploiting the fact that we only have dependence on r , the equation is reduced to:

$$\frac{1}{r} \frac{\partial}{\partial r} \left(r \frac{\partial V}{\partial r} \right) = \frac{1}{\pi R(z)^2} e^{-\frac{r^2}{R(z)^2}}.$$

By integrating twice with respect to r , we get the expression for the potential:

$$V(r, z) = a - \frac{Ei\left(-\frac{r}{R(z)^2}\right)}{4\pi} + b \log(r)$$

where Ei is the special function, called Exponential-Integral function, defined as:

$$Ei(r) = \int_{-r}^{\infty} \frac{e^{-t}}{t} dt.$$

The integration constants a is just a global constant which doesn't change the physics, we can choose it to be zero. The other constant b , is rather fixed by requiring a potential which is always non-singular, i.e. we impose a compensation between the singularity of the Ei function and the one of the logarithm at the origin. We obtain consequently:

$$V(r, z) = -\frac{Ei\left(-\frac{r}{R(z)^2}\right)}{4\pi} + \frac{\log(r)}{2\pi}. \quad (2.12)$$

We show in fig. (2.1), just to fix the ideas, the profile of the potential for the initial condition $R(z = 0) = 1$. To be more precise, we plot its opposite, since, in the optical frame it corresponds to the variation of refractive index in response to temperature. We can see how it has a maximum at the origin, where the laser is actually propagating and heating-up the medium consequently.

For how concerns the continuity equation, it is exactly solved by the velocity field $\vec{u}(\vec{r}, z) = \frac{\dot{R}(z)}{R(z)} \vec{r}$, as it can be easily checked by substitution. The phase function is therefore given by:

$$S(\vec{r}, z) = \frac{\dot{R}(z)}{2R(z)} r^2$$

where the dot denotes a derivative with respect to z . At this point we are able to write the Lagrangian of the system $L = \int \mathcal{L} d\vec{r}$, only as a function of $R(z)$ and $\dot{R}(z)$:

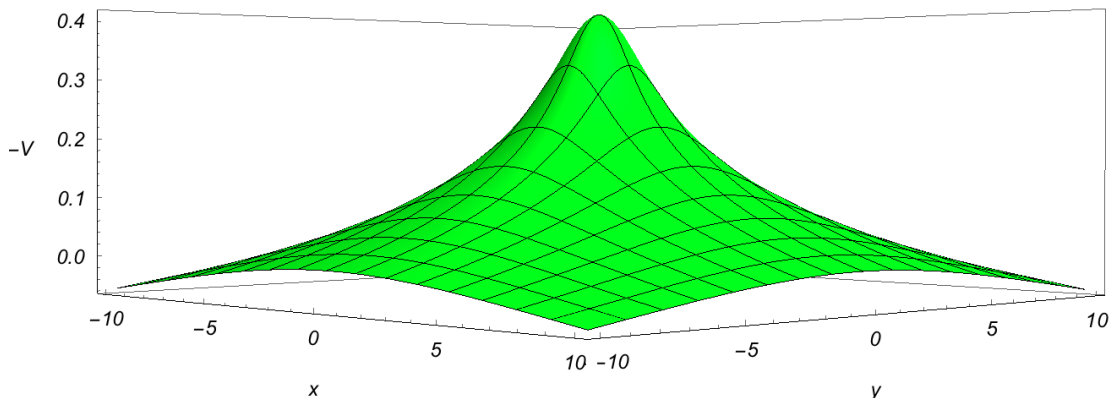


Figure 2.1. Plot of the opposite of the potential V , as described by Eq. (2.12), evaluated for $R(0) = 1$.

$$L(R, \dot{R}) = \frac{\dot{R}^2}{2} - \frac{1}{2R^2} - c \log R$$

where $c = \frac{1}{4\pi}$ is just a constant.

The Euler-Lagrange equation associated with this Lagrangian is:

$$\ddot{R} = \frac{1}{R^3} - \frac{c}{R} \quad (2.13)$$

which represents, in the Hamiltonian picture, the equation of motion of a point-like particle evolving in an external potential $U(R) = \frac{1}{2R^2} + c \log R$. Therefore, the first term on the right hand side of Eq. (2.13) is repulsive and associated with a kinetic pressure, important for small values of R , while the second term, which becomes important as R grows, is attractive and associated with gravity.

Eq. (2.13) can be solved analytically only for the inverse function $z(R)$, we don't discuss the details of the method since it's not in the purposes of this work, besides the so obtained solution $z(R)$ cannot be inverted analytically. However this result will be used for further comparisons (see 4.3.1).

As one last comment regarding this variational approach, it is important to underline how with the Gaussian ansatz 2.11, we are supposing to know exactly the dependence of the solution with the transverse spatial coordinates and we are additionally including the z dependence with the R function. This is why we integrated the Lagrangian density \mathcal{L} and we worked directly

with the Lagrangian L , because the informations about the \vec{r} dependence are already contained in the ansatz itself. The reason why this is a variational method is because, among all the possible gaussian solutions of the form of (2.11), the one whose width obeys to Eq. (2.13) is the one which minimizes the action of the system. However in principle the exact solution could have a completely different form; in the experimental framework we often deal with gaussian beams though, so it's still useful to consider such a variational model as we expect the solution to be not so different from a Gaussian at the beginning of the dynamics.

Part II

Numerical simulations

Chapter 3

Algorithm description

Equation (1.5) together with (1.6) represent a highly nonlinear problem, whose solutions can only be obtained through numerical techniques. In this chapter we describe the algorithm employed, which essentially consists into a second order method combined with a spectral method.

3.1 Split-Step method

In order to solve Eq. (1.1) or (1.5) we exploited a second order method, known as Split-Step method.

In general, this method can be applied whenever we deal with an equation like:

$$\frac{\partial\psi(\vec{r}, t)}{\partial t} = \hat{D}\psi(\vec{r}, t)$$

where \hat{D} is a differential operator, which can be split in two terms:

$$\hat{D} = \hat{F} + \hat{R}.$$

We will stick to the hat notation in order to describe differential operators.

The splitting is usually done in such a way that the differential equations:

$$\begin{aligned} \frac{\partial\psi(\vec{r}, t)}{\partial t} &= \hat{F}\psi(\vec{r}, t) \\ \frac{\partial\psi(\vec{r}, t)}{\partial t} &= \hat{R}\psi(\vec{r}, t) \end{aligned} \tag{3.1}$$

can be easily solved. In this case, we can formally write:

$$\begin{aligned}\psi(\vec{r}, t) &= e^{\hat{F}t}\psi(\vec{r}, 0) \\ \psi(\vec{r}, t) &= e^{\hat{R}t}\psi(\vec{r}, 0)\end{aligned}\tag{3.2}$$

where the exponential makes sense only if interpreted as a series:

$$e^{\hat{D}t} = \sum_{n=1}^{\infty} t^n \frac{\hat{D}^n}{n!}.\tag{3.3}$$

The solutions (3.2) of (3.1) are exact as long as \hat{D} does not depend on time and $\hat{D}\psi(\vec{r}, t)$ is continuous with continuous derivatives. The assumptions according to which $\hat{D}\psi(\vec{r}, t) \in C^1$ is in our case true, as we are considering a physical system and the wave function together with its derivatives must be continuous; in our frame though, \hat{D} is time dependent and the solution is more complicated. However, as we will see next, such operator is usually evaluated over small steps where it can be assumed almost constant.

From Eq. (3.3) is possible to prove that:

$$e^{\hat{D}t} = e^{(\hat{F}+\hat{R})t} = e^{\hat{F}t}e^{\hat{R}t} + \mathcal{O}(t^2).\tag{3.4}$$

Therefore the method, applied in a time interval $[0, T]$, deals with subdividing the interval in N small steps of amplitude Δt and applying in each step the two operators separately:

$$\begin{aligned}\psi(\vec{r}, t_{k+1}) &= e^{\hat{F}\Delta t}e^{\hat{R}\Delta t}\psi(\vec{r}, t_k) \quad k \in \{0, 1, 2, \dots, N-1\}, \\ t_{k+1} &= t_k + \Delta t, \quad t_0 = 0, \quad t_{N-1} = T.\end{aligned}$$

3.1.1 Error

The error of this method is linked to the $\mathcal{O}(t^2)$ term in Eq. (3.4), also known as local truncation error (LTE). The LTE is zero in the case where \hat{F} and \hat{R} commute, i.e.:

$$[\hat{F}, \hat{R}] = \hat{F}\hat{R} - \hat{R}\hat{F} = 0$$

which, as we will see next, is not true in our case. It is possible though to reduce the LTE by considering the alternative splitting:

$$e^{\hat{D}t} = e^{\frac{\hat{F}}{2}t}e^{\hat{R}t}e^{\frac{\hat{F}}{2}t} + \mathcal{O}(t^3) = e^{\frac{\hat{R}}{2}t}e^{\hat{F}t}e^{\frac{\hat{R}}{2}t} + \mathcal{O}(t^3)$$

as can be easily proved by considering the series in Eq. (3.3) up to second order. This is called Symmetric Split-Step method and follows the ideas of other similar algorithms as the Leap-Frog one, often employed in molecular dynamics simulations [16].

Moreover, when many steps are applied successively, the algorithm efficiency can be increased by merging two consecutive iterations, yielding:

$$\psi(\vec{r}, t_{k+1}) = e^{\frac{\hat{F}}{2}\Delta t} e^{\hat{R}\Delta t} e^{\hat{F}\Delta t} e^{\hat{R}\Delta t} e^{\frac{\hat{F}}{2}\Delta t} \psi(\vec{r}, t_k).$$

Adaptation to PHE

In order to apply this algorithm to solve Eq. (1.1), we can identify \hat{D} with the Hamiltonian of the system, \hat{F} with the kinetic energy and \hat{R} with the potential energy operators. The latter, being given by Eq. (1.2) explicitly depends on time, therefore we should write, instead of Eq. (3.2):

$$\psi(\vec{r}, t) = e^{\int_0^t dt' \hat{R}(t')} \psi(\vec{r}, 0).$$

However, if we choose a time step small enough compared with the variation of the potential, the integral can reasonably be approximated as a product between the integrand and the step and Eq. (3.2) remains valid.

In this way we can evolve the wave function according to the usual quantum time evolution operator $\hat{U}(t, t_0 = 0) = e^{-i\hat{H}t}$, considering the kinetic \hat{K} and the potential \hat{V} contribute in the Hamiltonian \hat{H} separately. The advantage of this is that the \hat{K} and \hat{V} operators are local, respectively in Fourier and in real space:

$$\begin{aligned} \psi(\vec{r}, t + \Delta t) &= \mathcal{F}^{-1}[e^{-iK\Delta t} \tilde{\psi}(\vec{k}, t)] = \mathcal{F}^{-1}[e^{-i\frac{k^2}{2}\Delta t} \tilde{\psi}(\vec{k}, t)] \\ \psi(\vec{r}, t + \Delta t) &= e^{-iV\Delta t} \psi(\vec{r}, t) \end{aligned}$$

being $\tilde{\psi}(\vec{k}, t)$ the Fourier transform (FT) in \vec{r} of ψ , k^2 the modulus square of the wave vector, V the potential we are dealing with and \mathcal{F}^{-1} denotes the inverse FT.

Taking into account the mapping between Eq. (1.1) and Eq. (1.5), we obtain the following pseudo-code:

$$\begin{aligned} \varepsilon(\vec{r}_\perp, z + \frac{\Delta z}{2}) &= \mathcal{F}^{-1}[e^{-i\frac{k^2}{2}\frac{\Delta z}{2}} \tilde{\varepsilon}(\vec{k}, z)] \\ \varepsilon(\vec{r}_\perp, z + \Delta z) &= e^{i\Delta n(\vec{r}, z + \frac{\Delta z}{2})\Delta z} \varepsilon(\vec{r}_\perp, z + \frac{\Delta z}{2}) \end{aligned}$$

$$\varepsilon(\vec{r}_\perp, z + \Delta z) = \mathcal{F}^{-1}[e^{-i\frac{k^2}{2}\frac{\Delta z}{2}} \tilde{\varepsilon}(\vec{k}, z + \Delta z)].$$

Therefore at each iteration we first compute the FT of ε , evolve it in Fourier space for half step with the kinetic energy and then we inverse Fourier transform it, this step corresponds to the first one of the latter three equations and is also known as "drift". Then we evolve ε for a whole step by using the potential energy in real space, in what is traditionally called "kick", i.e. the second one of the latter three equations. Finally we do another "drift".

3.2 Spectral method

We have shown how to solve only one of the two coupled equations described by (1.12). In particular we still have to discuss the solution of the Poisson equation:

$$\nabla_\perp^2 \Delta n(\vec{r}_\perp, z) = -g |\varepsilon(\vec{r}_\perp, z)|^2.$$

To solve this equation we rely on a spectral method i.e. a method based on Fourier Transform. Indeed by switching to Fourier space in the transversal dimensions, the differential equation becomes:

$$\widetilde{\Delta n}(\vec{k}_\perp, z) = g \frac{\widetilde{|\varepsilon(\vec{k}, z)|^2}}{k^2}$$

where the tilde denotes the Fourier transform in \vec{r}_\perp . Therefore we can easily evaluate Δn in Fourier space and inverse Fourier transform it whenever we need it.

In order to perform all of these FTs, we will exploit the algorithm described in the next section.

3.2.1 Fast Fourier Transform

The Fast Fourier Transform (FFT) algorithm computes the discrete Fourier Transform (DFT) of a function, in an efficient way. If one consider the definition of the DFT of a N dimensional vector $\vec{x} = (x_1, x_2, \dots, x_{N-1})$:

$$X_k = \sum_{n=0}^{N-1} x_n e^{-\frac{2\pi i n}{N} k} \quad k \in \{0, 1, 2, \dots, N-1\} \quad (3.5)$$

and devise the algorithm by simply applying it, the number of operations needed for the computation is $\mathcal{O}(N^2)$. Nevertheless, because of the symmetry of the DFT it is possible to divide the sum (3.5) of N terms into two sums of $\frac{N}{2}$ terms each:

$$X_k = \sum_{n=0}^{N/2-1} x_{2n} e^{-\frac{2\pi i n}{N/2} k} + e^{\frac{2\pi i k}{N}} \sum_{n=0}^{N/2-1} x_{2n+1} e^{-\frac{2\pi i n}{N/2} k}$$

by separating the contributes of the index even and odd values. This allows us to compute the DFT recursively in $\mathcal{O}(N \log N)$ operations and is known as Cooley-Tukey FFT algorithm.

We will employ this technique to evaluate the Fourier Transforms which appears in the Split-Step method as well, in particular we will exploit the FFTW library [17].

Chapter 4

Results for different initial conditions

The simulation was run with a discretization of the $x - y$ plan in a grid of $N \times N$ cells, with $N = 2048$, in such a way that the relation between the steps in real and Fourier space is:

$$\Delta k = \frac{2\pi}{N\Delta x}.$$

The step of the z axis was chosen to be 10^{-5} in order to ensure energy conservation.

As initial condition, we work with one or more gaussian beams of the form:

$$\varepsilon(\vec{r}_\perp, z = 0) = \mathcal{N}e^{-\frac{r_\perp^2}{R^2}}$$

where \mathcal{N} is fixed by the normalization and R is the width of the beam. Of course we made sure that the wavefunction is approximately zero at the boundaries of our grid during the entire simulation.

4.1 Parameters value

Since $|\varepsilon|^2$ is the intensity of the beam, its dimensions are:

$$[\varepsilon] = [E]L^{-2}R^{-1}$$

energy over a surface over a time, therefore its integral on the whole transversal plane coincides with the power of the beam. We consequently fixed the normalization in such a way that:

$$\iint dx dy |\varepsilon|^2 = P$$

where P is the power of the optical beam. At this point it is reasonable to adimensionalize Eq. (1.10) by choosing R as typical transversal dimension and $\sqrt{\frac{P}{R^2}}$ as typical amplitude of the beam. In this way, the control parameter g in Eq. (1.12) is given by:

$$g = \frac{\alpha\beta}{\kappa} k k_0 R^2 P. \quad (4.1)$$

The numerical values of these parameters, typical of the experimental framework are listed in table 4.1.

Parameters	Values
α	0.01 cm^{-1}
β	$14 \times 10^{-6} \text{ K}^{-1}$
κ	$0.7 \text{ W m}^{-1} \text{ K}^{-1}$
λ	532 nm
n_b	1.8
R	$360 \text{ }\mu\text{m}$
P	$1 - 10 \text{ W}$

Table 4.1. Values of the parameters one typically employ in an experimental setup.

where we recall that $k = k_0 n_b = n_b \frac{2\pi}{\lambda}$.

4.2 Conserved quantities

In order to test the code, we first checked that total energy and total probability (or, to be more precise, the power) are conserved, i.e. the quantities:

$$E = \langle \hat{H} \rangle_\varepsilon = \langle -\frac{1}{2k} \nabla_\perp^2 - \frac{1}{2} \Delta n \rangle_\varepsilon$$

$$\iint dx dy |\varepsilon|^2 = P$$

should be independent of z , which play the roles of time in our analogy. In the latter the $\langle \hat{\mathcal{O}} \rangle_\varepsilon$ denotes the quantum average of the operator $\hat{\mathcal{O}}$

over the wave function ε :

$$\langle \hat{O} \rangle_\varepsilon = \iint dx dy \varepsilon^* \hat{O} \varepsilon.$$

We expect that power is always perfectly conserved, as the the Split-Step method does not perturb the norm of the wave function, while on the other hand energy should be better conserved as the z step gets smaller. As pointed out by fig. 4.1 and 4.2 we verified that our algorithm correctly conserves the discussed quantities.

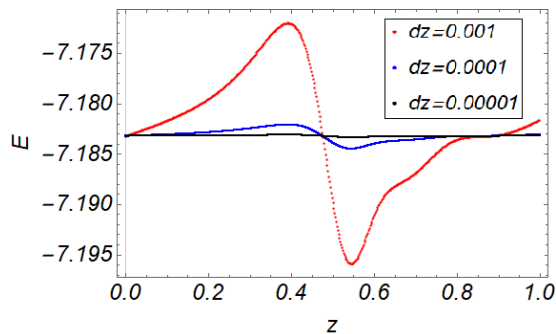


Figure 4.1. Total energy E as a function of the propagation length z , for several step sizes. As we can see for $dz = 10^{-5}$ we have good conservation.

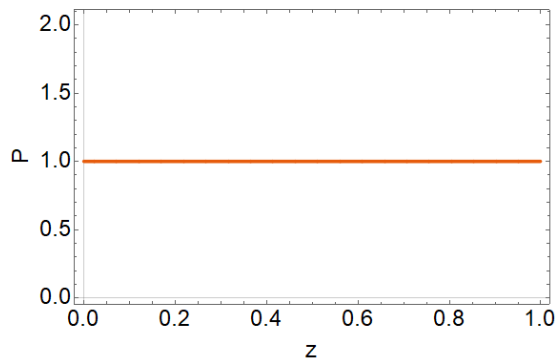


Figure 4.2. Total power P of the optical beam as a function of the propagation length z , as expected is it perfectly conserved.

4.3 Single beam initial condition

In fig. 4.3 and 4.4 is shown the output of the simulation for a single gaussian beam of power $P = 1.6W$. As we can see we have a self-focalisation at the beginning, due to the fact that the interaction is indeed attractive as we have a minus sign in Eq. (1.6), followed by non linear breathing modes, whose sizes get smaller as the laser keep propagating trough the medium.

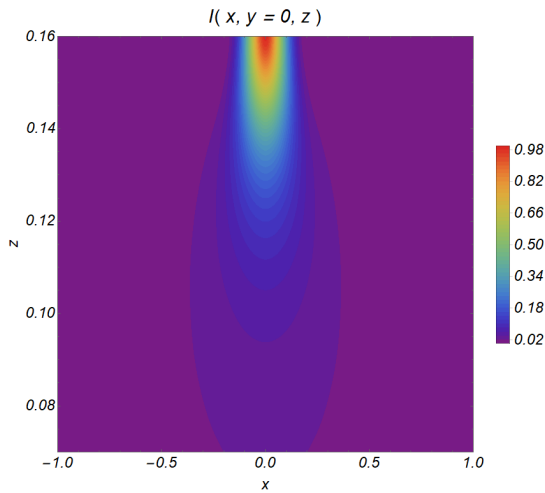


Figure 4.3. Initial evolution of the $y = 0$ slice of the normalized intensity of the optical beam as a function of x and z . The axis units are in the adimensional frame.

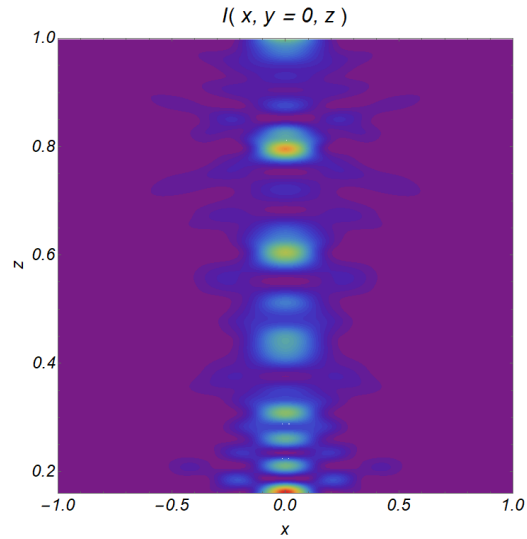


Figure 4.4. Evolution of the $y = 0$ slice of the normalized intensity of the optical beam as a function of x and z for larger values of z . The axis units are in the adimensional frame.

4.3.1 Variational model comparison

We are now able to compare the results of the numerical solutions of the equations with the one found according to the variational approach described in 2.2. In particular we compare the average width of the wave function $\langle x^2 + y^2 \rangle_{\varepsilon}$, with the solution of Eq. (2.13). As we can see from the comparison in fig. 4.5, we have good agreement in the initial phase of the dynamics, then we have a difference between the two curves which grows as z increases. There are essentially two reasons for that, even though they can be seen as the two sides of the same coin:

1. The Gaussian ansatz we made to derive the Lagrangian approach is not the exact solution of the equations.
2. As z grows, other phenomena like Landau damping and violent relaxation, start to play an import role. This phenomena are typical of such systems characterized by long range interactions and will be better explained in the next chapter.

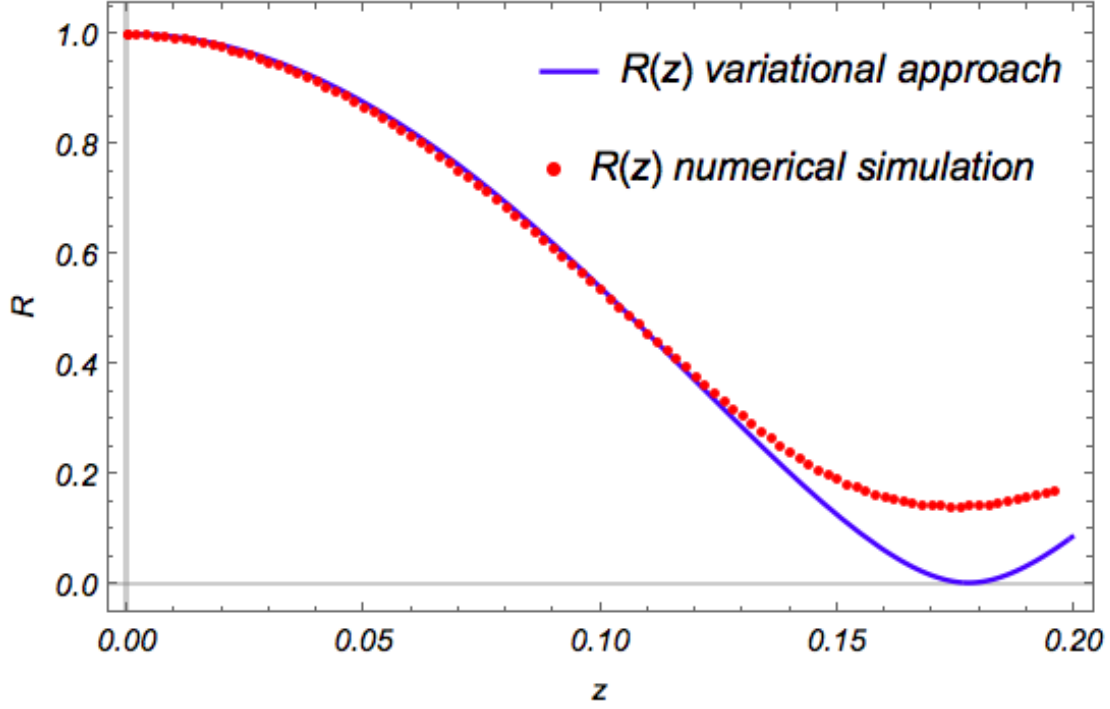


Figure 4.5. Comparison between the exact solution of the equation for R coming from the variational model and the one obtained with the numerical simulation. All the units are in the adimensional frame.

4.4 Double beam initial condition

We also run the simulation by inserting a double gaussian as initial condition:

$$\varepsilon(\vec{r}_\perp, z = 0) = \mathcal{N} \left(e^{-\frac{(|\vec{r}_\perp + \vec{a}|)^2}{R^2}} + e^{-\frac{(|\vec{r}_\perp - \vec{a}|)^2}{R^2}} \right)$$

where again the normalization constant \mathcal{N} was chosen to be consistent with the total power of the injected beams and the parameter \vec{a} was fixed in such a way that we have no relevant overlapping between the beams at the beginning, i.e. $|\vec{a}| > 3R$. We show in fig 4.6 the plot of the numerical solution of the equations for such initial condition.

As we can see there is a merging of the beams in the first phase of the dynamics, due again to the fact that the interaction is self-focusing, then there is a repulsion which is essentially linked to diffraction effect and finally as the propagation length increases the two beams merge again.

Since the dynamics showed from these simulations is very rich, it would be

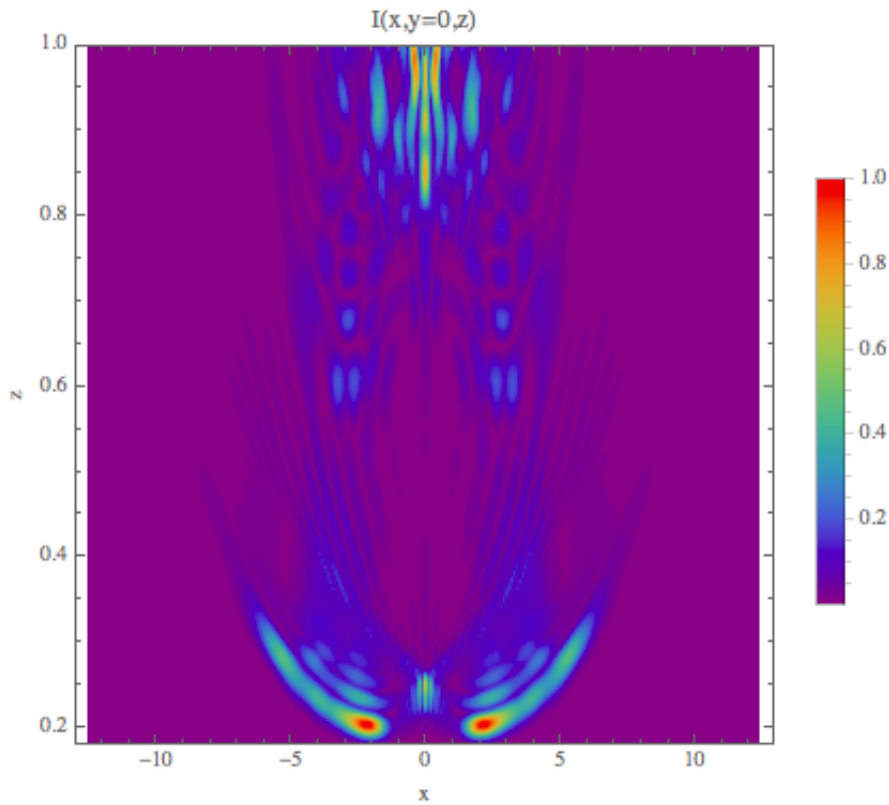


Figure 4.6. Evolution of the $y = 0$ slice of the normalized intensity of the optical beam as a function of x and z for a double gaussian initial condition. All the units are in the adimensional frame.

interesting to directly compared these results with the evolution of optical wavepackets observed in the experiments, we plan to do that in a future cooperation with the INPHYNI lab.

Chapter 5

Quasi-stationary state

In the previous chapter we mentioned that the system, for large values of z is dominated by the Landau damping phenomenon as well as by a violent relaxation. Now we are going to explain this in details and we are going to discuss how the system reaches a quasi-stationary state.

5.1 Virial theorem

The Landau damping phenomenon is strongly linked to the Virial theorem, we start from its explanation in the classical case and then focus on the quantum version, which is the interesting one for our system.

5.1.1 Classical Virial theorem

In the classical case, for the analogue gravitational system in dimension $d = 3$, after sufficiently long time a stationary state is reached. This state is described by the Virial theorem, which in its classical version states that for such a system twice the time average of the kinetic energy computed over a long period, is equal to the opposite of the potential energy, averaged over the same period:

$$2\bar{K} = -\bar{U}.$$

Phenomenologically, Landau damping deals with the violent dynamics of the system in the beginning, which gets more violent then smaller the virial ratio $\frac{K}{2|U|}$ is at the initial time. The kinetics energy starts to rapidly and intensively oscillate, whit an amplitude which slowly decreases as time grows, relaxing progressively to the stationary state predicted by the theorem.

5.1.2 Quantum Virial theorem

For a quantum system characterized by the same interactions, happens more or less the same. The quantum Virial theorem [18] indeed states that, if the system is in an eigenstate of the Hamiltonian, the average of the kinetic energy over the wave function of the system is equal to half the average of the potential energy:

$$\langle 2\hat{K} \rangle_{\varepsilon} = - \langle \hat{\vec{r}} \cdot \nabla \hat{V} \rangle_{\varepsilon} . \quad (5.1)$$

Note that in the quantum version of the theorem, the two sides of the equation are not averaged over time, therefore they are exactly the same, the system must be in an eigenstate of the Hamiltonian though.

In the particular case of our system, it is possible to evaluate the right hand side of Eq. (5.1) by exploiting $G(\vec{r}, \vec{r}')$, the Green function of the 2-dimensional Laplace operator (see Appendix B):

$$\begin{aligned} G(\vec{r}, \vec{r}') &= \frac{1}{2\pi} \log |\vec{r} - \vec{r}'| \\ \hat{V} = -\Delta n(\vec{r}, z) &= g \int G(\vec{r}, \vec{r}') |\varepsilon(\vec{r}', z)|^2 d\vec{r}' = \\ &= \frac{g}{2\pi} \int \log |\vec{r} - \vec{r}'| |\varepsilon(\vec{r}', z)|^2 d\vec{r}' . \end{aligned}$$

Consequently, after some manipulation (see Appendix B) we find the value to which the kinetic energy relaxes:

$$\langle \hat{K} \rangle = \frac{g}{8\pi} \quad (5.2)$$

where g is out control parameter, given by Eq. (4.1).

5.2 Comparison with simulations

Coming back to the simulation, we now compare the behaviour of the kinetic energy obtained for different initial conditions, with the relaxation values predicted by the quantum Virial theorem. In this case, we set a single Gaussian initial condition and vary the power associated with the beam, in particular we explored values of power very similar to the one we are able to work with experimentally: 1W, 1.5W, 3W and 5W. As we initialize the system to a state which is not stationary at all, since simple gaussian beams are not

solutions of Eq. (1.5) and (1.6), we expect the kinetic energy to fluctuate around the predicted value.

From fig. 5.1, we can see how in all cases we get good agreement within a discrepancy of the order of 5% (see table 5.1), it is possible to observe though, how this discrepancy get smaller as the power increases. One reason for that is that by increasing the power, we are decreasing the Virial ratio $K/\frac{g}{8\pi}$, as the power of the beam is inside U (see Eq. 4.1), therefore the relaxation is faster. However, a more insightful way to understand this, is explained in the next section.

P (W)	d (%)
1	8.2
1.5	4.7
2	4.1
3	3.7
5	2.8

Table 5.1. Values of the percentage discrepancy d between the average of K and the Virial value for different initial conditions.

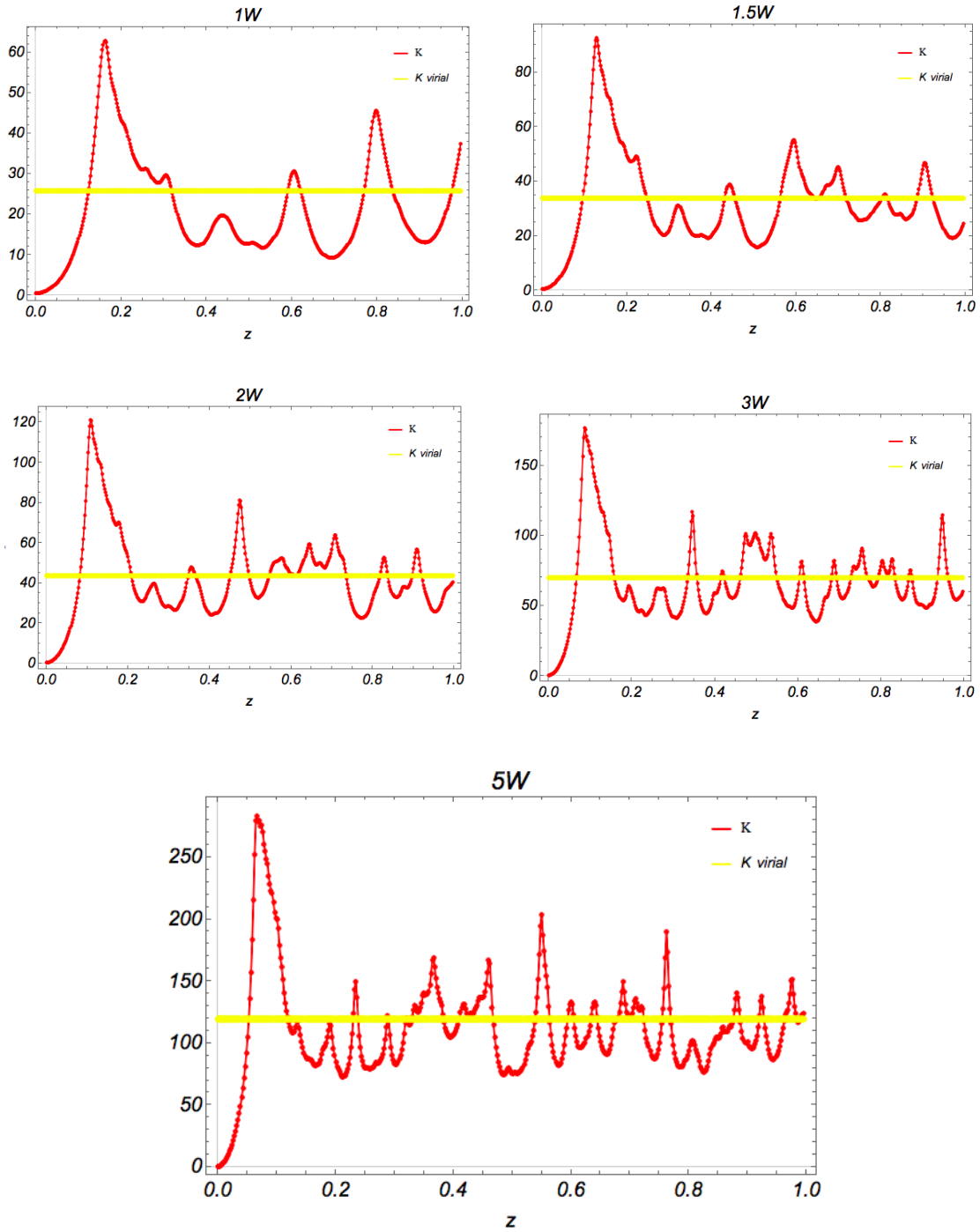


Figure 5.1. Plots of the kinetic energy as function of the propagation direction z in the adimensional frame, together with the Virial relaxation value for different powers of the optical beam.

5.2.1 Multiscale nature of the problem

Qualitatively speaking, one reason why larger values of power lead to a faster formation of a quasi-stationary state, is that increasing the power means increasing the interaction size of the system, therefore we expect the self-focalisation to be faster. Indeed considering Eq. (4.1), points out how g , which is the coupling parameter associated with the interaction, is proportional to the power of the beam. Under a quantitative point of view, this can be understood by pointing out the multiscale nature of the NSE system. This system is indeed characterized by two scales for the propagation length z , one linked to the kinetic pressure and the other one linked with the self-focusing interaction. In order to underline the first scale we mentioned, we can rely on the adimensionalization of the equations. By setting the typical scales for ε and the transversal lengths, i.e. x and y , in a way compatible with the experimental set:

$$\widetilde{\nabla}_{\perp}^2 = \frac{1}{l_{typ}^2} \nabla_{\perp}^2 = \frac{1}{R^2} \nabla_{\perp}^2$$

$$|\widetilde{\varepsilon}|^2 = \varepsilon_{typ}^2 |\varepsilon|^2 = \frac{P}{R^2} |\varepsilon|^2$$

exactly like we already did in section 4.1, this leads to having just one control parameter, given by Eq. (4.1), in the adimensionalized equations:

$$i \frac{\partial \varepsilon}{\partial z} + \frac{1}{2} \nabla_{\perp}^2 \varepsilon + \Delta n \varepsilon = 0$$

$$\nabla_{\perp}^2 \Delta n = -g |\varepsilon|^2.$$

Therefore, if we look at the typical scale of the propagation length z_{typ} , given by Eq. (1.11), it will be:

$$z_{typ} = \frac{1}{k_0 \Delta n_{typ}} = k R^2.$$

As k is associated in the original dimensionful frame with the kinetic energy term, this is the kinetic pressure scale.

On the other hand, if we consider Eq. (1.6) and exploit its green function solution form (see Appendix B):

$$\Delta n(\vec{r}, z) = \frac{\alpha \beta}{2\pi \kappa} \int d\vec{r}' \log(|\vec{r} - \vec{r}'|) |\varepsilon(\vec{r}', z)|^2$$

we get that the self-focusing interaction scale is given by:

$$\Delta n_{typ} = \frac{\gamma R^2 \varepsilon_{typ}}{2\pi} = \frac{P\gamma}{2\pi}$$

where for simplicity of notation we denoted $\gamma = \frac{\alpha\beta}{\kappa}$. Therefore the typical value of the propagation length associated with the interaction term is:

$$z_{typ} = \frac{1}{k_0 \Delta n_{typ}} = \frac{2\pi}{P\gamma k_0} = \frac{\lambda}{P\gamma} \quad (5.3)$$

which indeed decreases as the power grows.

5.3 Study of the stationarity in time

Together with the quasi-stationary state related to the propagation length, there exist also a stationary state in time. Until now we have considered the system to be in such a stationary regime, as we ran all the simulations by considering the heat-like equation to be time independent. In principle, in the experimental optical system, we deal with these two equations though:

$$\begin{aligned} i \frac{\partial \varepsilon}{\partial z} + \frac{1}{2k} \nabla_{\perp}^2 \varepsilon + k_0 \Delta n \varepsilon &= 0 \\ \frac{\rho_0 C}{\kappa} \frac{\partial \Delta n}{\partial t} &= \nabla_{\perp}^2 \Delta n + \frac{\alpha\beta}{\kappa} |\varepsilon|^2 \end{aligned} \quad (5.4)$$

where the second Eq. in (5.4) is a direct consequence of (1.9) and we remember that $\rho_0 C$ is the heat capacity per unit volume of the optical medium. We know that by waiting for sufficiently long time, heat propagation in the optical medium will saturate and the system will reach a stationary regime described by Eq. (5.4) with the l.h.s of the refractive index equation approximately equal to zero. To investigate the details of this limit, in principle one should study the unicity of the solutions of this two coupled differential equations system. However, we proceeded with a method perhaps not as much elegant, but still efficient, namely we went for a numerical solution.

5.3.1 Numerical solution

The algorithm employed is essentially the same we described in chapter 3, with the difference that now we should consider one more loop over time. The initial conditions are:

$$\varepsilon(\vec{r}_\perp, z = 0, t = 0) = \mathcal{N}e^{-\frac{r_\perp^2}{R^2}}$$

$$\Delta n(\vec{r}_\perp, z, t = 0) = 0$$

as we always inject a gaussian beam and assume that at $t = 0$ the refractive index of the medium remains unchanged, since no propagation has occurred yet. In addition, we require the following boundary condition:

$$\varepsilon(\vec{r}_\perp, z = 0, t) = \varepsilon(\vec{r}_\perp, z = 0, t = 0) \quad \forall t > 0$$

since at the beginning of the medium interface, i.e. $z = 0$, we force the solution to be gaussian.

Adimensionalization

In order to make Eq. (5.4) adimensional, we follow the usual procedure we already exploited in section 4.1, with particular attention to the fact that we have one extra term. The result is very similar though:

$$i\frac{\partial \varepsilon}{\partial z} + \frac{1}{2}\nabla_\perp^2 \varepsilon + \Delta n \varepsilon = 0$$

$$\frac{\partial \Delta n}{\partial t} = \nabla_\perp^2 \Delta n + g|\varepsilon|^2$$

where g is again given by (4.1). For how concerns the typical time scale, it turns out to be:

$$\alpha_t = \frac{\rho_0 C R^2}{\kappa}$$

therefore, since in our experimental setup the heat capacity per unit volume of the medium is $\rho_0 C = 1.6 \frac{J}{K cm^3}$, we have $\alpha_t \approx 0.5s$.

Results

We ran the simulation with the same spatial steps we used in the stationary one and with a time step $\Delta t = 0.001$. In order to study the convergence of the solution, we made several snapshots of the intensity of the single gaussian beam $|\varepsilon|^2$ and compared them with the output of the time independent simulation with the same initial conditions. The results are shown in fig. 5.2

and points out the system actually converges to the same state, in a time which is of the order of some α_t .

Therefore, we expect the time transient to last approximately a few seconds in the experiment. It will be interesting to check whether this is true or not in practice, as well as performing a mathematical study of the unicity of solutions regarding Eq. (5.4), all of this will be done in the PhD thesis which will continue this project.

5.3 – Study of the stationarity in time

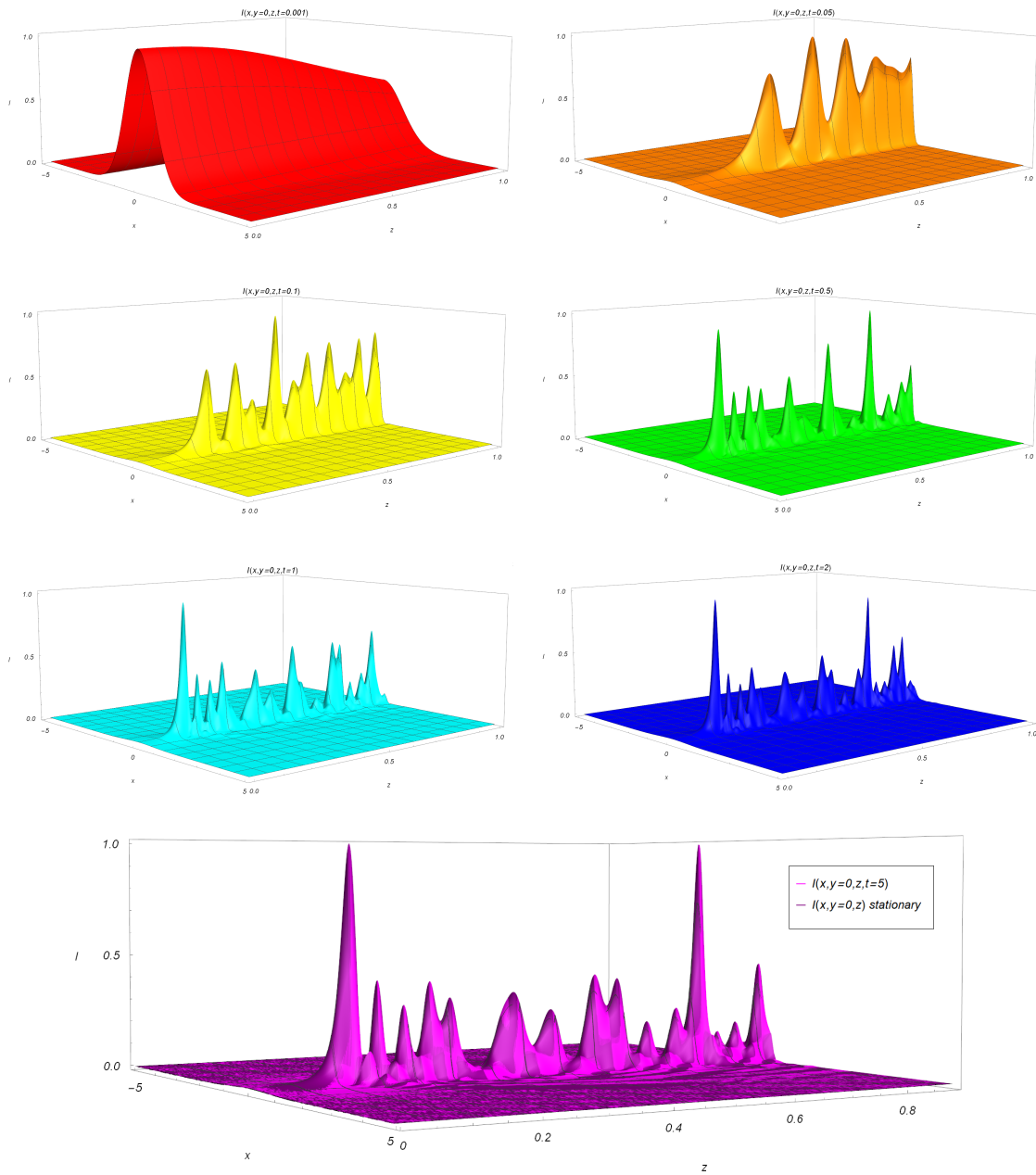


Figure 5.2. Plots of the $y = 0$ slice of the normalized intensity of the optical beam as a function of x and z for different values of time. The last plot shows an overlap with the time stationary solution. All the units are in the adimensional frame.

Chapter 6

Phase-space picture

In this chapter, we are going to focus on the phase-space picture of the NSE, by introducing the Husimi distribution [19].

6.1 Classical limit of NSE

The employment of a phase-space picture could seem not appropriate for a quantum system, for which knowing simultaneously the values of position and momentum is forbidden by Heisenberg uncertainty relation. However, the optical system we are dealing with can actually be considered as classical. There are at least two ways to realise it.

6.1.1 Comparison with Planck constant

The first one deals with a direct comparison between the PHE and the NSE:

$$i\frac{\partial\varepsilon}{\partial z} + \frac{1}{2k}\nabla_{\perp}^2\varepsilon + k_0\Delta n\varepsilon = 0.$$

Formally the PHE can be interpreted as a Schrödinger equation for a particle of mass k , in a universe where $\hbar = 1$. However, $k \approx 10^8$ in our setup, since we are working with beams in the visible region of the electromagnetic spectrum, this is like considering a quantum particle with a huge mass. More quantitatively, by comparing the uncertainty relations for an electron and for our optical system:

$$\begin{aligned}\Delta x_e &\approx 10^{-10}m & \Delta p_e &= m\Delta v_e \approx 10^{-30}kg \times 10^6ms^{-1} \\ \Delta x_e\Delta p_e &\approx \hbar \approx 10^{-34}Js\end{aligned}$$

$$\Delta x \approx 10^{-4}m \quad \Delta p \approx 10^8 m^{-1}$$

$$\Delta x \Delta p \gg 1.$$

We can see that the typical scales of our optical system are much larger than the analogue value of \hbar , compared with what usually happens for an electron in a hydrogen atom (we used the values of the electron typical position and momentum delocalization, Δx_e and Δp_e , given by the Bohr model.)

Momentum interpretation in the optical framework

In the latter we treated the momentum in the PHE equation as a wavenumber, this is due to the De Broglie relation $\vec{p} = \hbar \vec{k}$ together with the fact that in our analogy, as we have already mentioned, $\hbar = 1$. Therefore, is completely legit to interpret the momentum \vec{p} as a wavevector in the optical framework: its magnitude will be fixed by the wavelength of the laser we are injecting, but its component will in principle vary with the propagation length. In addition, as $\Delta x \Delta p$ must have the dimension of \hbar which again is 1 in this picture, it is easy to convince ourselves that p must indeed have the dimension of the inverse of a length, therefore, of a wavenumber.

6.1.2 Role of the quantum pressure

The second reason, is linked with the quantum pressure term $\frac{1}{2} \nabla \cdot \left(\frac{\nabla^2 \sqrt{\rho}}{\sqrt{\rho}} \right)$, we have introduced at the end of section 2.1. It is possible to show how for our optical system this term is actually very small compared with the others appearing in Eq. (2.7), proving that in the experimental context we are actually dealing with a classical system, as one expect. The comparison between the quantum pressure term and all the other ones in the Euler-like equation, is shown in figure 6.1.

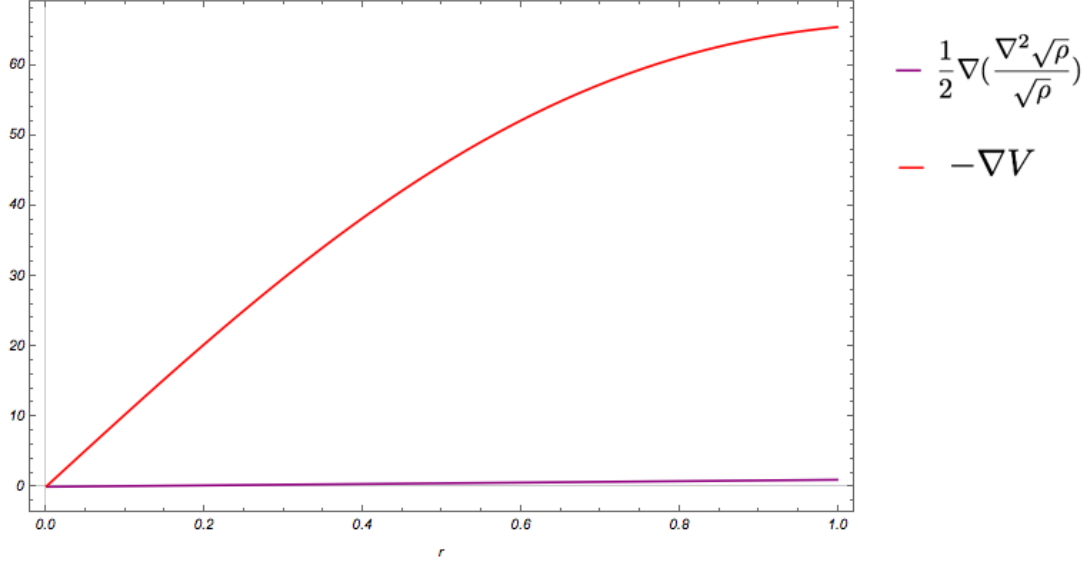


Figure 6.1. Plot of the quantum pressure term (purple curve), compared with the self-focusing potential term (red curve), appearing in Eq. (2.7) as a function of the distance from the origin in the transverse plane in units of the beam width.

6.2 Husimi distribution

Now, that we have justified why we would like to rely on a phase-space representation of this system, we present the mathematical tool we will exploit in order to achieve the goal: the Husimi distribution $F(\vec{r}, \vec{p})$. It is defined as follows:

$$F(\vec{x}, \vec{p}, t) = \left| \left(\frac{1}{2\pi\hbar} \right)^{n/2} \left(\frac{1}{\pi\eta^2} \right)^{n/4} \int d^m r \psi(\vec{r}, t) \exp \left[-\frac{(\vec{x} - \vec{r})^2}{2\eta^2} - i \frac{\vec{p} \cdot (\vec{r} - \vec{x}/2)}{\hbar} \right] \right|^2 \quad (6.1)$$

where n denotes the dimension of the space where the system represented by the wavefunction ψ lives, therefore in our optical case we will take $n = 2$. As we can see from Eq. (6.1), we are essentially doing a spatial coarse graining over a scale η with a gaussian field and then performing something which is very similar to a Fourier Transform in momentum to the coarse grained wavefunction. The parameter η must be chosen in a proper way, depending on the scales of the problem, in particular it must satisfy [22]:

$$d \ll \eta \ll \Delta x \quad (6.2)$$

where d is the grid step we employ in the numerical simulation and Δx the typical delocalization of the system, therefore in the case of the optical beam, its width.

Such a phase-space probability density is by construction always non-negative, it doesn't give back the right values of current and charge densities when integrated though [23], this is why it is actually a quasi-probability distribution. To be more specific, by considering the one dimensional case for simplicity:

$$\int dp F(x, p, t) \neq |\psi(x, t)|^2$$

$$\int dp F(x, p, t) p \neq j(x)$$

where $|\psi(x, t)|^2$ and $j(x) = \frac{\hbar}{2mi}(\psi^* \frac{\partial \psi}{\partial x} - \psi \frac{\partial \psi^*}{\partial x})$ are what traditionally in quantum mechanics are called and interpreted as charge and current density respectively [24].

6.2.1 Numerical evaluation and plots

In evaluating numerically the Husimi distribution (HD), we exploited again the FFT algorithm, this allows to save a lot of computational time: in particular we switch from N^3 operations required by an algorithm which applies directly the definition of the HD according to Eq. (6.1), to $\mathcal{O}(N^2 \log N)$ operations with the FFTW. We computed the HD in the optical framework, for different values of the propagation length z , which substitutes time in the definition (6.1). We then plotted $F(x, y = 0, p_x, p_y = 0, z)$, for different values of z , making sure that, as one expect, the radial symmetry proper of the wavefunction is maintained. The radial symmetry implies the odd-like symmetry: $F(x, y = 0, p_x, p_y = 0, z) = F(-x, y = 0, -p_x, p_y = 0, z)$.

What is happening in the plots of fig. 6.2 is that at $z = 0$ the system has $p_x = 0$, and a gaussian-like distribution in x , consistently with our initial gaussian beam condition. The reason why we have zero "velocity" at the beginning is that, as explained in section 6.1.1, the momentum can actually be interpreted as the wavevector, therefore p_x coincides with its components in the x direction, which is zero at the beginning since we are injecting the beam in a perpendicular way with respect to the medium transversal face.

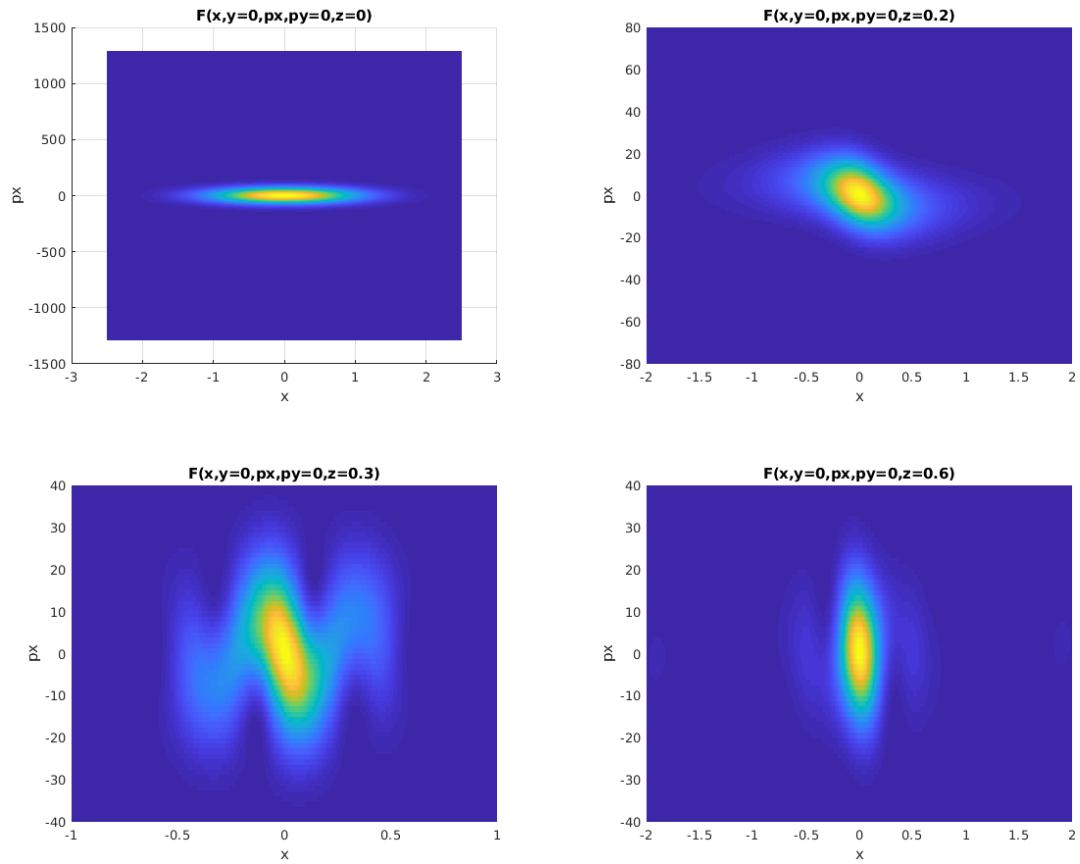


Figure 6.2. Plots of the Husimi density function $F(x, y = 0, p_x, p_y = 0)$, in the slice $y = 0 = p_y$ for $z = 0, 0.2, 0.3, 0.6$, in natural units.

For how concerns the $z > 0$ plots, we can rely on the gravitational analogy in order to understand them in a more intuitive way. For example for $z = 0.1$ the particles start to collapse towards the centre: in the $x > 0$ they therefore acquire a negative momentum and in the $x < 0$ region a positive one, notice how the odd-like symmetry is indeed satisfied. In general the plots points out a filamentation in phase-space which is typical of long range interactions systems.

Conclusions

We have shown that, with a proper mapping, a medium with positive thermal–optical nonlinearity can be exploited in order to simulate the NSE. The simulations pointed out how the system, after a quite rapid and violent behavior represented from the first peak of the kinetic energy as a function of z , slowly relaxes to a quasi-stationary state characterized by smaller oscillations. Energy and power conservation have been verified, the variational gaussian model turned out to be valid only for in the initial part of the dynamics, while the agreement with the Virial theorem is good for high powers. We also showed that exploring the system for larger values of z leads to better agreement, anyhow in the experimental framework is better to manipulate the power and keep the length of the material constant. This is due to the fact that firstly, very long material with these optical properties are not easy to produce and secondly, then longer the medium is, then larger will be the effect of power dissipation. There are still many things which need to be done about this project and they will be carried out with a PhD thesis. For how concerns the theoretical aspects, we aim to better understand some mathematical properties of the NSE equations, like the unicity of solutions and its classical limit with the Vlasov-Poisson equation [20]. Moreover we would like to perform some studies about the breaking of symmetry [21] and the structure formations in the cosmological context, starting from slightly asymmetrical initial conditions and analysing how they evolve in space and time. Since the problem is very challenging numerically, requiring the resolution of a wide range of spatial scales to keep the symplectic properties of the dynamics, there is a lot of work to do concerning algorithmic developments: optimization, adaptive grids, smart time steps and implementation on GPUs. Finally for how concerns direct observations, there will be a cooperation with the experimentalists of the INPHYNI lab who will perform experiments on the nonlinear optical system, validating and refining the model.

Appendices

Appendix A

Details of the PHE derivation

The slowly varying part of the nonlinear polarization is given by:

$$\vec{P}_{NL}(\vec{r}, t) \approx \epsilon \epsilon_{NL} E(\vec{r}, t)$$

where the nonlinear contribution to the dielectric constant is defined as:

$$\epsilon_{NL} = \frac{3}{4} \chi_{xxxx}^{(3)} |\vec{E}(\vec{r}, t)|^2.$$

Since the linear part of the polarization can be written as $\vec{P}_L(\vec{r}, t) = \epsilon \chi_{xx}^{(1)} E(\vec{r}, t)$, we can provide the following expression for the dielectric constant:

$$\tilde{\epsilon}(\omega) = 1 + \chi_{xx}^{(1)}(\omega) + \epsilon_{NL}$$

where a tilde denotes a Fourier Transform of the quantity under it. The dielectric constant can be used to define the refractive index \tilde{n} and the absorption coefficient $\tilde{\alpha}$ which both become intensity dependent because of ϵ_{NL} . It is customary to introduce:

$$\tilde{n} = n_0 + n_2 |E|^2 \quad \tilde{\alpha} = \alpha_0 + \alpha_2 |E|^2.$$

The linear index n_0 and the absorption coefficient α are related respectively to the real and imaginary part of $\chi_{xx}^{(1)}$. Using $\epsilon = (\tilde{n} + \frac{i\tilde{\alpha}c}{2\omega_0})^2$, Eq. (1.8), the nonlinear, or Kerr, coefficient n_2 and the two-photon absorption coefficient α_2 are given by:

$$n_2 = \frac{3}{8n} \text{Re}(\chi_{xxxx}^{(3)})$$

$$\alpha_2 = \frac{3\omega_0}{4nc} \text{Im}(\chi_{xxxx}^{(3)})$$

which shows how the nonlinear part of the refractive index is linked to the nonlinear part of \vec{P} .

Appendix B

Evaluating Virial integral

In order to evaluate the quantity which appears on the r.h.s of Eq. (5.1), we first need to compute \hat{V} in a suitable form. To do that we exploit the Green function of the 2d Laplacian operator, i.e. the function G which satisfies:

$$\nabla^2 G(\vec{x}; \vec{y}) = \delta(|\vec{x} - \vec{y}|). \quad (\text{B.1})$$

Since the problem is rotationally symmetric about the special point \vec{y} , the fundamental solution can only depend on the scalar distance from that point:

$$G(\vec{x}; \vec{y}) = G(|\vec{x} - \vec{y}|).$$

Because of the delta function, we can easily integrate both sides of Eq. (B.1), in particular we do that on the following domain:

$$B_r = \{\vec{x} \in \mathbb{R}^2 : |\vec{x} - \vec{y}| < r\}.$$

Therefore, we have, by applying the divergence theorem and the definition of directional derivative:

$$\begin{aligned} 1 &= \int_{B_r} dV \nabla^2 G = \int_{\partial B_r} dS \hat{n} \cdot \nabla G = \\ &= \int_{\partial B_r} d\Omega \frac{\partial G}{\partial r} r = 2\pi r \frac{dG}{dr} \end{aligned}$$

which by comparing each sides yields:

$$\frac{dG}{dr} = \frac{1}{2\pi r}$$

this equation once integrated shows us that the Green function of the 2d Laplacian operator is a logarithm.

We can therefore write:

$$\begin{aligned}
 \langle -\vec{r} \cdot \nabla \hat{V} \rangle &= \langle \vec{r} \cdot \nabla (\Delta n(\vec{r}, z)) \rangle = \\
 &= g \langle \int \vec{r} \cdot \nabla G(\vec{r}, \vec{r}') |\varepsilon(\vec{r}', z)|^2 d\vec{r}' \rangle = \\
 &= \frac{g}{2\pi} \iint \frac{\vec{r} \cdot (\vec{r} - \vec{r}')}{|\vec{r} - \vec{r}'|^2} |\varepsilon(\vec{r}', z)|^2 |\varepsilon(\vec{r}, z)|^2 d\vec{r}' d\vec{r}.
 \end{aligned}$$

By the changing $\vec{r} \leftrightarrow \vec{r}'$ and exploiting the identity $\vec{r} \cdot (\vec{r} - \vec{r}') + \vec{r}' \cdot (\vec{r}' - \vec{r}) = |\vec{r} - \vec{r}'|^2$, together with the normalization of ε , we finally get:

$$\langle -\vec{r} \cdot \nabla \hat{V} \rangle = \frac{g}{4\pi}.$$

Therefore:

$$\langle \hat{K} \rangle = \frac{g}{8\pi}.$$

Bibliography

- [1] Campa, A., Dauxois, T. and Ruffo, S., 2009. *Statistical mechanics and dynamics of solvable models with long-range interactions*. Physics Reports, 480(3-6), pp.57-159.
- [2] Levin, Y., Pakter, R., Rizzato, F.B., Teles, T.N. and Benetti, F.P., 2014. *Nonequilibrium statistical mechanics of systems with long-range interactions*. Physics Reports, 535(1), pp.1-60.
- [3] Bekenstein, R., Schley, R., Mutzafi, M., Rotschild, C. and Segev, M., 2015. *Optical simulations of gravitational effects in the Newton–Schrödinger system*. Nature Physics, 11(10), p.nphys3451.
- [4] Roger, T., Maitland, C., Wilson, K., Westerberg, N., Vocke, D., Wright, E.M. and Faccio, D., 2016. *Optical analogues of the Newton–Schrödinger equation and boson star evolution*. Nature communications, 7, p.13492.
- [5] Bernal, A. and Guzman, F.S., 2006. *Scalar field dark matter: Nonspherical collapse and late-time behavior*. Physical Review D, 74(6), p.063504.
- [6] Widrow, L.M. and Kaiser, N., 1993. *Using the Schrödinger equation to simulate collisionless matter*. The Astrophysical Journal, 416, p.L71.
- [7] Schive, H.Y., Chiueh, T. and Broadhurst, T., 2014. *Cosmic structure as the quantum interference of a coherent dark wave*. Nature Physics, 10(7), p.496.
- [8] Giulini, D. and Großardt, A., 2012. *The Schrödinger–Newton equation as a non-relativistic limit of self-gravitating Klein–Gordon and Dirac fields*. Classical and Quantum Gravity, 29(21), p.215010.
- [9] *An Introduction to Quantum Field Theory*, M. E. Peskin & D. V. Schröder, Westview Press.
- [10] Kivshar, Y.S. and Agrawal, G., 2003. *Optical solitons: from fibers to photonic crystals*. Academic press.
- [11] Saleh, B.E., Teich, M.C. and Saleh, B.E., 1991. *Fundamentals of photonics (Vol. 22)*. New York: Wiley.
- [12] Boyd, R.W., 2003. *Nonlinear optics*. Elsevier.

- [13] Navarrete, A., Paredes, A., Salgueiro, J.R. and Michinel, H., 2017. *Spatial solitons in thermo-optical media from the nonlinear Schrödinger-Poisson equation and dark-matter analogs*. Physical Review A, 95(1), p.013844.
- [14] E. Madelung, *Quantum Theory in Hydrodynamical Form*. Zeit. f. Phys., 40 (1927), 322.
- [15] Manfredi, G., Hervieux, P.A. and Haas, F., 2013. *Variational approach to the time-dependent Schrödinger-Newton equations*. Classical and Quantum Gravity, 30(7), p.075006.
- [16] Berendsen, H.J., Postma, J.V., van Gunsteren, W.F., DiNola, A.R.H.J. and Haak, J.R., 1984. *Molecular dynamics with coupling to an external bath*. The Journal of chemical physics, 81(8), pp.3684-3690.
- [17] Frigo, M. and Johnson, S.G., 1999. *FFTW user's manual*. Massachusetts Institute of Technology.
- [18] Zhao, Q., Faizal, M. and Zaz, Z., 2017. *Short distance modification of the quantum virial theorem*. Physics Letters B, 770, pp.564-568.
- [19] K. Husimi, Nippon Sugaku-Buturigakkwai Kizi Dai 3 Ki 22, 264 (1940).
- [20] Mocz, P., Lancaster, L., Fialkov, A., Becerra, F. and Chavanis, P.H., 2018. *Schrödinger-Poisson-Vlasov-Poisson correspondence*. Physical Review D, 97(8), p.083519.
- [21] Sylos Labini, F., Benhaiem, D. and Joyce, M., 2015. *On the generation of triaxiality in the collapse of cold spherical self-gravitating systems*. Monthly Notices of the Royal Astronomical Society, 449(4), pp.4458-4464.
- [22] Manfredi, G., Hervieux, P.A. and Haas, F., 2013. *Variational approach to the time-dependent Schrödinger-Newton equations*. Classical and Quantum Gravity, 30(7), p.075006.
- [23] Colomés, E., Zhan, Z. and Oriols, X., 2015. *Comparing Wigner, Husimi and Bohmian distributions: which one is a true probability distribution in phase space?*. Journal of Computational Electronics, 14(4), pp.894-906.
- [24] Rossetti, C., 2011. *Rudimenti di meccanica quantistica*. Levrotto & Bella.